Bioelectric Gene and Reaction Networks: Supporting Information

July 19, 2017

Alexis Pietak and Michael Levin

Allen Discovery Center at Tufts University, Medford, MA, USA

Bioelectricity-integrated gene and reaction networks (BIGR) were modeled using the BioElectric Tissue Simulation Engine (BETSE) software program. Details regarding discretization of equations and computational grids can be found elsewhere [1]. BETSE has been extended, allowing creation of user-defined substances, the construction of regulatory network models by specifying regulatory relationships between substances, substance participation in standard chemical reactions, substance transmembrane transport reactions, and to allow a substance to gate ion channels and modulate the activity of other model elements such as gap junctions. The following supplies theoretical details relating to model details, ion channel, ion pump and transporter dynamics, and BIGR network models presented in the main text.

Contents

1 Model Details

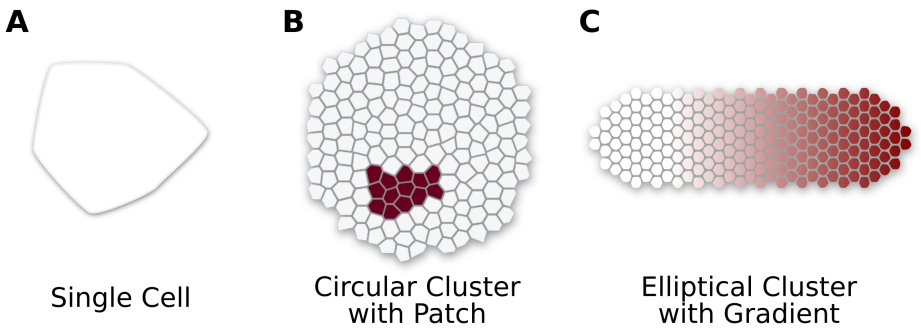

Figure 1: The general forms of geometric models explored in this work. Model geometries included: single cell models (panel A); a circular cell cluster of variable number of gap junction connected cells, one cell layer in thickness, with an internal patch of cells (red cells in B) in which V_{mem} is different in the patch due to a difference in the sodium to potassium membrane permeability ratio ($P^{Na}_{mem} : P^{K}_{mem}$) for cells in the patch (panel B); and an elliptical cell cluster of variable number of gap junction connected cells, one cell layer in thickness, with an initial condition of an asymmetric concentration of a specific chemical substance (panel C).

Model Geometries

As shown in Fig 1, simulations utilized three different classes of model geometries: (1) single cell models were used to explore fundamental relationships between V_{mem} and cytosolic concentrations defined in regulatory networks (Fig 1A); (2) the direct, instructional influence of V_{mem} on regulatory network state and associated positional information profiles was explored using a circular shaped cell cluster with an internal patch of cells (red cells in B) in which a transient V_{mem} perturbation was applied by temporarily altering the ratio of the sodium to potassium membrane permeability ratio ($P^{Na}_{mem} : P^{K}_{mem}$); and (3) emergent V_{mem} regenerative dynamics and patterning were explored in simulations using an elliptical cell cluster, which has a small, initial asymmetric concentration of a chemical substance (panel C). Cell clusters were constructed from a randomly perturbed hexagonal lattice of seed points which were used to construct a Voronoi diagram, and contained from 1 to 500 cells (models measuring 20 to 500 μm in length).

Model Initial Ion Concentrations

The initial value of ion concentration inside cells and in the environment are summarized in Table 1. Initial values in the extracellular space were also used as a fixed concentration applied to the global boundaries. Simulations begin with net charge in cells and the environment equal to zero and V_{mem}=0.0 mV.

A summary of commonly used symbols and constants is provided in Table 2.

Ion	Intracellular ($\frac{mol}{m^3}$)	Extracellular ($\frac{mol}{m^3}$)
Na^+	8.0	145.0
K^+	125.0	5.0
Cl^-	20.0	105.0
Ca^{2+}	1.0e^{-4}	1.0
HCO_3^-	13.0	36.0
P^-	100.0	10.0
H^+	4.0e^{-5}	4.0e^{-5}
ATP^{2-}	2.5	0.0
ADP^{1-}	0.15	0.0
Pi^{1-}	0.15	0.0

Table 1: Initial values of default concentration inside cells and in the environment used for all simulations.

Symbol	Description	Value	Units
F	Faraday Constant	96,485	$\frac{C}{mol}$
R	Gas Constant	8.3145	$\frac{J}{K\,mol}$
T	Temperature	310	K
i	Substance index		
V_{mem}	Transmembrane potential		mV
Φ_i	Chemical flux of substance i		$\frac{mol}{m^2\,s}$
r_b	Rate of reaction b		$\frac{mol}{s}$
$[A]$	Concentration of substance A		$\frac{mol}{m^3}$
z_i	Charge of substance i		
P_i	Membrane permeability to substance i		$\frac{m}{s}$
$\triangle G^o$	Change in Gibb's free energy under standard conditions		$\frac{J}{mol}$
K_{eqm}	Equilibrium constant for reaction		
K_i	Half-max rate constant for substance i		$\frac{mol}{m^3}$
μ_i	Electrochemical potential of substance i		$\frac{J}{mol}$

Table 2: A summary of mathematical symbols and constants commonly used in the supplementary material.

2 Defining Equations of BIGR Networks

Ion pumps and transporters were modeled as reactions occurring across membranes. The equilibrium constant for the ion pump or transporter reaction was stated in terms of the standard Gibbs free energy change:

$$K_{eqm} = exp\left(-\frac{\triangle G^o}{R\,T}\right) \tag{1}$$

The definition for free energy change of a general chemical reaction was taken as [2]:

$$\triangle G = \sum_{prod_i} a_i \mu_i - \sum_{react_j} a_j \mu_j \tag{2}$$

However, instead of chemical potential, the *electrochemical* potential of each reactant or product was utilized, which assumed voltage to be zero outside of the cell, meaning the voltage inside the cell was equivalent to the value of V_{mem}:

$$\mu_i = \mu_o + z_i\,F\,V \tag{3}$$

2.1 Specific transporter/ion pump models

Organic Cation Transporter OCT3

The OCT3 is a facilitated transporter for cationic monoamines such as serotonin and acetylcholine, and is found expressed outside of the brain [3–5]. The overall reaction utilized for the OCT3 transporter moving serotonin ($5HT^+$) was:

$$5HT^+_{env} \leftrightarrows 5HT^+_{cell} \tag{4}$$

The electrochemical potential for $5HT^+$ inside and out of the cell was defined using Eq 3, the reaction free energy change was estimated using Eq 2, and using the definition of the reaction equilibrium constant from Eq 1, the transporter equilibrium constant was expressed as:

$$K_{eqm} = exp\left(\frac{-z_{5HT}\,F\,V_{mem}}{R\,T}\right) \tag{5}$$

with $z_{5HT} = 1.0$.

Note that Eq 5 embodies the logical premise that transport of a positively charged substance from the environment to the cell is more favorable for a negative V_{mem}, and vice-versa for negatively charged substances. Consistently, the reverse direction of transport out of the cell to the environment is favored for negatively charged substances moving from the environment to the cell with more negative V_{mem}.

The final rate expression for the flux from the reversible OCT3 transporter is:

$$\Phi_{OCT3} = \Phi_{OCT3}^{max} \left(\left(\frac{\left(\frac{[5HT_{env}]}{K_f^{5HTenv}} \right)}{1 + \left(\frac{[5HT_{env}]}{K_f^{5HTenv}} \right)} \right) - \left(\frac{\frac{[5HT_{cell}]}{[5HT_{env}]}}{exp(-z_{5HT}\, F\, V_{mem}/R\, T)} \right) \left(\frac{\left(\frac{[5HT_{cell}]}{K_r^{5HT_{cell}}} \right)}{1 + \left(\frac{[5HT_{cell}]}{K_r^{5HT_{cell}}} \right)} \right) \right) \tag{6}$$

with $\Phi_{OCT3}^{max} = 1.0e^{-8}\, mol/m^2 s$, $K_f^{5HT_{env}} = 1.0e^{-3}\, mol/m^3$, $K_r^{5HT_{cell}} = 1.0e^{-2}\, mol/m^3$.

Consistent with the above model, the OCT3 transporter has been experimentally found to be V_{mem} sensitive [5].

Sodium-potassium adenosine triphosphatase ion pump Na^+/K^+-ATPase

The overall reaction utilized for the Na^+/K^+-ATPase pump was:

$$3\, Na_{cell}^{+} + 2\, K_{env}^{+} + ATP_{cell}^{2-} \leftrightarrows 3\, Na_{env}^{+} + 2\, K_{cell}^{+} + ADP_{cell}^{-} + Pi_{cell}^{-} \tag{7}$$

Using Eq 2, the overall free energy, ΔG_{pump}, for the Na^+/K^+-ATPase pump reaction was expressed:

$$\triangle G_{pump} = \triangle G_{ATP}^{o} + R\, T\, ln\,(Q) - F\, V_{mem} \tag{8}$$

The reaction quotient of the pump was expressed (with substance concentrations converted to mol/L):

$$Q = \frac{[ADP_{cell}]\,[Pi_{cell}]\,[Na_{env}]^3\,[K_{cell}]^2}{[ATP_{cell}]\,[Na_{cell}]^3\,[K_{env}]^2} \tag{9}$$

Using Eq 5 an expression for the Na^+/K^+-ATPase pump reaction equilibrium constant in terms of the standard free energy for ATP hydrolysis and cell V_{mem} is:

$$K_{NaKATP}^{eqm} = exp\left(\frac{-\triangle G_{ATP}^{o} + F\,V_{mem}}{R\,T}\right) \tag{10}$$

where $\triangle G_{ATP}^{o} = -36.0e^{3}\,J/mol$ was utilized.

An estimate for the rate of the reversible enzymatic pump reaction follows as:

$$\Phi_{NaKATP} = \Phi_{NaKATP}^{max}\left(r_f - \frac{Q}{K_{eqm}} r_r\right) \tag{11}$$

where:

$$r_f = \frac{\frac{cATP}{K_{ATP}}\left(\frac{cNa_{in}}{K_{Na}}\right)^3\left(\frac{cK_{out}}{K_K}\right)^2}{\left(1+\frac{cATP}{K_{ATP}}\right)\left(1+\left(\frac{cNa_{in}}{K_{Na}}\right)^3\right)\left(1+\left(\frac{cK_{out}}{K_K}\right)^2\right)} \tag{12}$$

$$r_r = \frac{\frac{[ADP]}{K_{ADP}}\frac{[Pi]}{K_{Pi}}\left(\frac{[Na_{out}]}{K_{Nao}}\right)^3\left(\frac{[K_{in}]}{K_{Ki}}\right)^2}{\left(1+\frac{[ADP]}{K_{ADP}}\right)\left(1+\frac{[Pi]}{K_{Pi}}\right) =, \left(1+\left(\frac{[Na_{out}]}{K_{Nao}}\right)^3\right)\left(1+\left(\frac{[K_{in}]}{K_{Ki}}\right)^2\right)} \tag{13}$$

Values for the constants $K_{Na} = 5.0\,mol/m^3$, $K_K = 0.2\,mol/m^3$ and $K_{ATP} = 0.15\,mol/m^3$ were obtained from [6]. Reverse reaction constants $K_{ADP} = 1.0\,mol/m^3$, $K_{Pi} = 1.0\,mol/m^3$, $K_{Nao} = 140.0\,mol/m^3$ and $K_{Ki} = 120.0\,mol/m^3$ were estimated. Values of $\Phi_{NaKATP}^{max} = 1.0e-7\,mol/m^2\,s$ were roughly calibrated to Na^+/K^+-ATPase pump rates reported for Xenopus oocytes ([7]).

The V_{mem}-sensitivity of the Na^+/K^+-ATPase ion pump (which is related to increased cytosolic Na^+ levels with V_{mem} depolarization via increased Na^+ membrane permeability), consistent with the above model, has been experimentally noted [8, 9].

Divalent metal transporter DMT1

The overall reaction utilized for the DMT1 transporter assumed the transporter to be functioning in an H^+-independent transport modality, valid for pH 7.4 of the modeling context [10], and was:

$$Fe_{env}^{2+} \leftrightarrows Fe_{cell}^{2+} \tag{14}$$

Following the same theoretical process as used for pumps and transporters discussed previously, the final rate expression for the flux from the reversible DMT1 transporter was described by:

$$\Phi_{DMT1} = \Phi^{max}_{DMT1} \left(\left(\frac{\left(\frac{[Fe_{env}]}{K_f}\right)}{1 + \left(\frac{[Fe_{env}]}{K_f}\right)} \right) - \left(\frac{\frac{[Fe_{cell}]}{[Fe_{env}]}}{exp(-z_{Fe}\, F\, V_{mem}/R\, T)} \right) \left(\frac{\left(\frac{[Fe_{cell}]}{K_r}\right)}{1 + \left(\frac{[Fe_{cell}]}{K_r}\right)} \right) \right) \quad (15)$$

with $z_{Fe} = 2.0$, $Fe^{max}_{DMT1} = 5.0e^{-8}\, mol/s\, m^2$, $K_f = 0.6e^{-3}\, mol/m^3$, $K_r = 1.0e^{-2}\, mol/m^3$, approximately based on the parameters of the H^+-uncoupled Fe^{2+} transport mechanism described by Mackenzie et al. [10].

The V_{mem}-sensitivity of the DMT1 transporter consistent with the above model has been experimentally noted [10].

Sodium-dependent serotonin transporter SERT

The overall reaction utilized for the SERT transporter was:

$$Na^+_{env} + 5HT^+_{env} + Cl^-_{env} + K^+_{cell} \leftrightarrows Na^+_{cell} + 5HT^+_{cell} + Cl^-_{cell} + K^+_{env} \quad (16)$$

Following the same theoretical process described for other reversible pumps and transporters described above, the flux from the SERT transporter was described as:

$$\Phi_{SERT} = \Phi^{max}_{SERT} \left(r_f - \frac{Q}{K_{eqm}} r_r \right) \quad (17)$$

Where:

$$Q = \frac{[Na_{cell}]\,[5HT_{cell}]\,[Cl_{cell}]\,[K_{env}]}{[Na_{env}]\,[5HT_{env}]\,[Cl_{env}]\,[K_{cell}]} \quad (18)$$

$$K_{eqm} = 1.0 \quad (19)$$

$$r_f = \frac{\left(\frac{[Na_{cell}]}{K_{Na}}\right)\left(\frac{[5HT_{cell}]}{K_{5HT}}\right)\left(\frac{[Cl_{cell}]}{K_{Cl}}\right)\left(\frac{[K_{env}]}{K_K}\right)}{(1 + \frac{[Na_{cell}]}{K_{Na}})\,(1 + \left(\frac{[5HT_{cell}]}{K_{5HT}}\right))\,(1 + \left(\frac{[Cl_{cell}]}{K_{Cl}}\right))\,(1 + \left(\frac{[K_{env}]}{K_K}\right))} \quad (20)$$

$$r_r = \frac{\left(\frac{[Na_{env}]}{K_{Nao}}\right)\left(\frac{[5HT_{env}]}{K_{5HTo}}\right)\left(\frac{[Cl_{env}]}{K_{Clo}}\right)\left(\frac{[K_{cell}]}{K_{Ko}}\right)}{(1+\frac{[Na_{env}]}{K_{Nao}})\,(1+\left(\frac{[5HT_{env}]}{K_{5HTo}}\right))\,(1+\left(\frac{[Cl_{env}]}{K_{Clo}}\right))\,(1+\left(\frac{[K_{cell}]}{K_{Ko}}\right))} \tag{21}$$

Where $\Phi_{5HT}^{max} = 5.0e-8\, mol/m^2s$, $K_{Na} = 1.0\ mol/m^3$, $K_{5HT} = 1.0e^{-3}\ mol/m^3$, $K_{Cl} = 1.0\ mol/m^3$, $K_K = 1.0\ mol/m^3$, $K_{Nao} = 1.0\ mol/m^3$, $K_{5HTo} = 1.0e^{-2}\ mol/m^3$, $K_{Clo} = 1.0\ mol/m^3$, and $K_{Ko} = 1.0\ mol/m^3$, all parameters estimated.

The V_{mem}-sensitivity of the SERT transporter under conditions of low extracellular Cl^- and absence of Cl^- related transporters, consistent with the above model, has been experimentally reported [11, 12].

2.2 Specific Ion channel Models

In BETSE, the behavior of any ion channel is handled by determining how the membrane permeability for specific ions (P_i^{chan}) is altered by the activity of the ion channel, and in turn effects on transmembrane flux by ion channel activity may affect V_{mem}, as described in the main text. For all K^+ channel models described below, $z_K = 1.0$.

KCNK9 and "K+ Channel" Potassium Leak Channels

Here the KCNK9 is taken as a specific example of a K^+ channel with minimal voltage sensitivity, although a number of potassium leak channels exist in the tandem pore domain K^+ channel family [13]. Potassium leak channels are also referred to as simply "K^+ Channel" in the main text, and are equivalent to the KCNK9 channel model. The K^+ flux for the KCNK9 or "K^+ Channel" is modeled assuming that the channel has a fixed K^+ membrane permeability $P_K^{KCNK9} = P_K^{KChannel} = 5.0e^{-8}\, m/s$:

$$\Phi_K^{KCNK9} = \frac{z_K\, V_{mem}\, F\, P_K^{KCNK9}}{R\, T}\left(\frac{c_K^{cell} - c_K^{env}\, exp\left(-\frac{z_K V_{mem} F}{RT}\right)}{1 - exp\left(-\frac{z_K V_{mem} F}{RT}\right)}\right) \tag{22}$$

While the tandem pore domain K^+ leak channel family channels have minimal voltage sensitivity, they are subject to regulation by a wide range of potential substances [13–15], which may be accounted for in BIGR network models.

Kir2.1 Inward Rectifying Potassium Channel

The Kir2.1 channel was modeled in terms of a voltage-sensitive cytosolic Mg^{2+} ion block of the channel [16, 17], using the following formula to describe channel activity:

$$\Phi_K^{Kir2.1} = \frac{z_K\, V_{mem}\, F\, P_K^{Kir2.1}}{R\, T}\left(\frac{c_K^{cell} - c_K^{env}\, exp\left(-\frac{z_K V_{mem} F}{RT}\right)}{1 - exp\left(-\frac{z_K V_{mem} F}{RT}\right)}\right) \tag{23}$$

$$P_K^{Kir2.1} = P_K^{max}\left(\frac{1}{1 + \left(\frac{[Mg]}{K_{Mg}^{Kir2.1}}\right)}\right) \tag{24}$$

$$K_{Mg}^{Kir2.1} = K_{Mg}^{o}\, exp\left(\frac{-V_{mem}\, z_{Mg}^{eff}\, F}{R\, T}\right) \tag{25}$$

Here $P_K^{max} = 6.7e^{-10}\, m/s$, $[Mg] = 0.5\, mol/m^3$,$K_{Mg}^{o} = 0.025\, mol/m^3$, and $z_{Mg}^{eff} = 1.5$.

ATP-Sensitive Inward Rectifying Potassium Channel (K-ATP, Kir6.1, Kir6.2)

The ATP-sensitive K^+ Channels are inward rectifying potassium channels Kir6.1 and Kir6.2. In this work, we apply ATP co-regulation to the base model of Kir2.1, to obtain a K^+ flux component approximating the behavior of a K-ATP channel described by:

$$\Phi_K^{ATPKir} = \frac{z_K\, V_{mem}\, F\, P_K^{ATPKir}}{R\, T}\left(\frac{c_K^{cell} - c_K^{env}\, exp\left(-\frac{z_K V_{mem} F}{RT}\right)}{1 - exp\left(-\frac{z_K V_{mem} F}{RT}\right)}\right) \tag{26}$$

$$P_K^{ATPKir} = P_K^{max}\left(\frac{1}{1 + \left(\frac{[ATP]}{K_{ATP}^{ATPKir}}\right)^4}\right)\left(\frac{1}{1 + \left(\frac{[Mg]}{K_{Mg}^{ATPKir}}\right)}\right) \tag{27}$$

$$K_{Mg}^{ATPKir} = K_{Mg}^{ATPKir_o}\, exp\left(\frac{-V_{mem}\, z_{Mg}^{eff}\, F}{R\, T}\right) \tag{28}$$

Here $P_K^{max} = 6.7e^{-10}\, m/s$, $[Mg] = 0.5\, mol/m^3$,$K_{Mg}^{o} = 0.025\, mol/m^3$, and $z_{Mg}^{eff} = 1.5$ and $K_{ATP}^{ATPKir} = 1.0$.

K_V1.5 Voltage-Sensitive Potassium Channel

The delayed rectifier K_V1.5 calcium channel presented herein was based on the Hodgkin-Huxley style model of Philipson *et al.* [18], which defines m_{inf}, m_{tau} , h_{inf} and h_{tau} as four functions of V_{mem}:

$$\begin{aligned} m_{inf} &= 1.0/(1 + exp(-(V_{mem} + 6.0)/6.4)) \\ m_{tau} &= -0.1163\, V_{mem} + 8.33 \\ h_{inf} &= 1.0/(1 + exp((V_{mem} + 25.3)/3.5)) \\ h_{tau} &= -15.5\, V_{mem} + 1620.0 \end{aligned} \tag{29}$$

Where the parameters m and h change in time according to:

$$\begin{aligned} \frac{\partial m}{\partial t} &= \frac{m_{inf} - m}{m_{tau}} \\ \frac{\partial h}{\partial t} &= \frac{h_{inf} - h}{h_{tau}} \end{aligned} \tag{30}$$

And are used to modulate the membrane permeability to K^+ ions as:

$$P_K^{Kv1.5} = P_K^{max}\, m\, h \tag{31}$$

The Kv1.5 channel produces a component of transmembrane K^+ flux described by:

$$\Phi_K^{Kv1.5} = \frac{z_K\, V_{mem}\, F\, P_K^{Kv1.5}}{R\, T} \left(\frac{c_K^{cell} - c_K^{env}\, exp\left(-\frac{z_K V_{mem} F}{RT}\right)}{1 - exp\left(-\frac{z_K V_{mem} F}{RT}\right)} \right) \tag{32}$$

Here $P_K^{max} = 6.7e^{-9}\, m/s$.

Voltage Clamp simulations of the K_v1.5 channel model

We found that voltage-gated channels such as the Kv1.5, are highly dynamic, and that the I-V curves resulting from a particular simulated voltage clamp protocol can vary significantly in form. In our simulations, we found this to primarily be the case for the Kv1.5 channel model and not the KCNK or Kir channel models.

The primary voltage clamp protocol utilized to explore channel I-V curves in the main manuscript utilized a hold voltage that changed sequentially as a function of time, spending 2 seconds

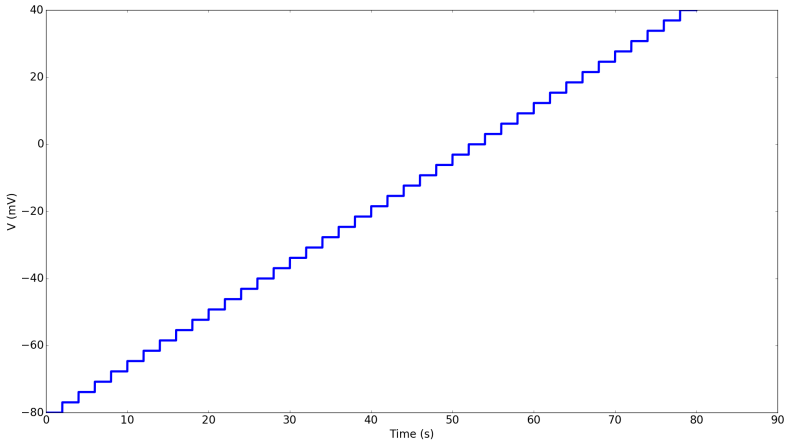

Figure 2: Hold voltage as a function of time for "primary" voltage clamp protocol used to study the steady-state behavior of ion channels discussed in the main text.

at each voltage in a series of voltages separated by 1 mV and running from -120 mV to + 40 mV. The temporal form of the voltage in our primary voltage clamp simulation assumed the form shown in Figure 2. The objective of our primary voltage clamp protocol was to investigate the true steady-state behavior of our modeled channels, in order to understand how these channels may alter resting V_{mem} in somatic systems.

Following a similar protocol to the one used in the experiments of McKay and Worley in [19] to obtain "instantaneous activation" I-V curves for Kv1.5 channels, in our simulations, we utilized a secondary voltage clamp protocol such that the hold voltage changed according to a duty cycle as a function of time, spending 2 seconds at -80 mV, followed by 0.1 s at a depolarized voltage in a series where a "recording" of K+ current was taken at the 0.1 s point, before returning the voltage to -80 mV. The temporal form of the voltage in our secondary "voltage clamp" simulation assumed the form shown in Figure 3.

Using both primary and secondary voltage clamp protocol to simulate the I-V curves of the Kv1.5 channel, we found that the primary voltage clamp protocol reproduced the expected steady-state behavior of the channel (Fig 4A), whereas the secondary voltage clamp protocol closely reproduced the form of the I-V curves obtained by McKay and Worley [19] (Fig 4B).

$Ca_V1.2$ calcium channel

The L-type $Ca_V1.2$ calcium channel was based on the model of Avery *et al.* [20], which defines m_{inf}, m_{tau} , h_{inf} and h_{tau} as four functions of V_{mem}:

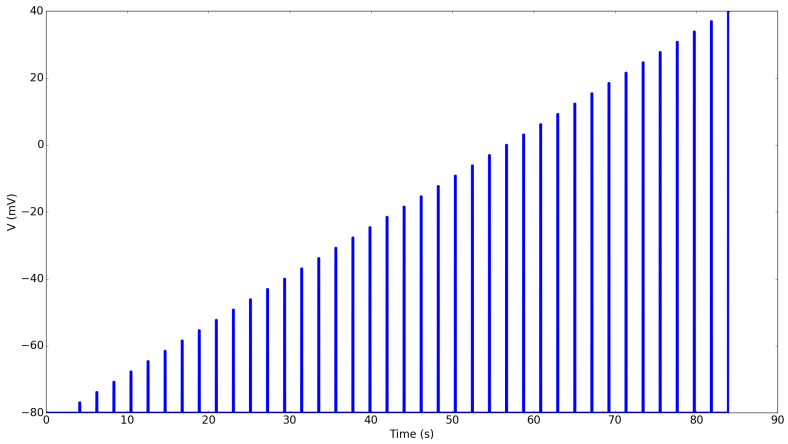

Figure 3: Hold voltage as a function of time for "secondary" voltage clamp protocol designed to follow the electrophysiology methods of McKay and Worley (2001) [19].

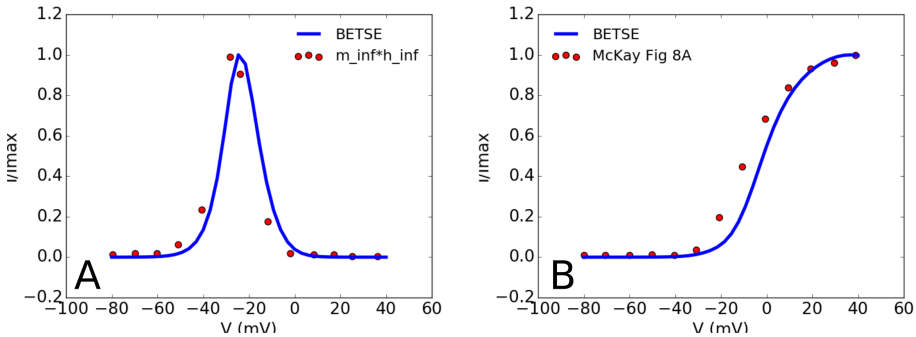

Figure 4: Different I-V curves are obtained for the Kv1.5 channel model when simulated using the "primary" voltage clamp protocol (panel A) or the "secondary" voltage clamp protocol (panel B). Red circle series in panel A represents a sampling of the 'm_inf*h_inf' series representing the Philipson et al Kv1.5 channel model's steady-state behavior (original curves are available from Channelpedia from http://channelpedia.epfl.ch/images/89.original). Red circle series in panel B represents experimental data points for the Kv1.5 channel instantaneous activation I-V curve obtained from the control data series of Figure 8A in McKay and Worley (2001) [19].

$$\begin{aligned} m_{inf} &= 1.0/(1 + exp((V_{mem} + 30.0)/-6)) \\ m_{tau} &= (5.0 + 20.0/(1 + exp((V_{mem} + 25.0)/5))) \\ h_{inf} &= 1.0/(1 + exp((V_{mem} + 80.0)/6.4)) \\ h_{tau} &= (20.0 + 50.0/(1 + exp((V_{mem} + 40.0)/7))) \end{aligned} \tag{33}$$

In BETSE we use these four functions to describe the membrane permeability to calcium ions as a function of time and V_{mem}, where:

$$\begin{aligned} \frac{\partial m}{\partial t} &= \frac{m_{inf} - m}{m_{tau}} \\ \frac{\partial h}{\partial t} &= \frac{h_{inf} - h}{h_{tau}} \end{aligned} \tag{34}$$

and:

$$P_{Ca}^{CaV1.2} = P_{Ca}^{max}\, m^2\, h \tag{35}$$

During each time-step, the membrane permeability would be updated according to Eqs 33, 34, 35 and the flux contribution for this specific channel would be calculated using:

$$\Phi_{Ca}^{CaV1.2} = \frac{z_{Ca}\, V_{mem}\, F\, P_{Ca}^{CaV1.2}}{R\, T} \left(\frac{c_{Ca}^{cell} - c_{Ca}^{env}\, exp\left(-\frac{z_{Ca} V_{mem} F}{RT}\right)}{1 - exp\left(-\frac{z_{Ca} V_{mem} F}{RT}\right)} \right) \tag{36}$$

Where $z_{Ca} = 2.0$ and $P_{Ca}^{max} = 1.0e^{-8}\, m/s$.

2.3 Metabolism

The Na^+/K^+-ATPase ion pump interfaces with cell metabolic processes via the hydrolysis of ATP. In all models, a very basic, irreversible metabolic reaction was utilized to replenish ATP consumed by the Na^+/K^+-ATPase ion pump:

$$ADP + Pi \rightarrow ATP \tag{37}$$

$$r_{metabolism} = r_{metabolism}^{max} \left(\frac{\frac{[ADP]}{K_{ADP}}}{1 + \frac{[ADP]}{K_{ADP}}} \right) \left(\frac{\frac{[Pi]}{K_{Pi}}}{1 + \frac{[Pi]}{K_{Pi}}} \right) \tag{38}$$

where $r_{metabolism}^{max} = 0.126\, mol/m^3\, s$, $K_{ADP} = 0.1\, mol/m^3$ and $K_{Pi} = 0.1\, mol/m^3$.

3 Network Models

3.1 Anterior-posterior polarity control network

The anterior-posterior polarity control network is a BIGR network describing the scale-invariant regeneration of an instructive V_{mem} depolarization, as described and analyzed in the main text.

Table 3 provides basic information about the additional substances included in the network model (i.e. substances added in addition to core ions, ATP and ADP that are present by default in all models with information listed in Table 1), Table 4 provides growth and decay expressions for each substance of the network model.

All equations for the anterior-posterior polarity control network model were programmatically generated from mathematical template equations on the basis of user-specified input data in the form of a BETSE configuration file. The configuration file that can be used with BETSE to run the anterior-posterior polarity control network is supplied as Supporting Information S2.

Substance	**Charge**	**GJ permeable?**	**Growth/decay?**	D_{GJ} **[m2/s]**	D_{mem} **[m2/s]**	**Initial** C_{cell} **[mM]**	**Initial** C_{env} **[mM]**
A	-2	True	True	$1.0e^{-12}$	0.0	0.0	0.0
B	0	True	True	$1.0e^{-12}$	0.0	0.0	0.0
X	0	False	False	0.0	0.0	0.5 (gradient)	0.0

Table 3: Substances of the anterior-posterior polarity control network. The general ions Na^+, K^+, Cl^-, Ca^{2+}, HCO_3^-, P^- , and the substances ATP, ADP and Pi were included in the model, with properties listed in Table 1.

Substance	**Activators**	**Inhibitors**	**Rate Equation**	**Parameters**
A	None	None	$r_A = r_A^{max} - \delta_A\,[A]$	$r_A^{max} = 2.5e^{-2}\,mol/m^3 s$ $\delta_A = 1.00e^{-2}\,mol/m^3 s$
B	'A'	None	$r_B = r_B^{max}\left(\frac{\left(\frac{[A]}{K_A}\right)^3}{1+\left(\frac{[A]}{K_A}\right)^3}\right) - \delta_B\,[B]$	$K_A = 0.50\,mol/m^3$ $r_B^{max} = 2.5e^{-2}\,mol/m^3 s$ $\delta_B = 2.5e^{-2}\,mol/m^3 s$

Table 4: Growth/decay expressions for the anterior-posterior polarity control network.

Channel	**Ions**	**Regulation**	**Channel Flux Expression**
K^+ channel	K^+	'B' and 'X'	$\frac{z_K V_{mem} F P_K^{KChannel}}{RT}\left(\frac{c_K^{cell} - c_K^{env} exp\left(-\frac{z_K V_{mem} F}{RT}\right)}{1-exp\left(-\frac{z_K V_{mem} F}{RT}\right)}\right)$ $P_K^{KChannel} = P_K^{max}\left(\frac{1}{1+\left(\frac{[B]}{K_B}\right)^3}\right)\left(\frac{1}{1+\left(\frac{[X]}{K_X}\right)}\right)$ $P_K^{max} = 1.33e-10\,m/s$, $K_B = 0.5\,mol/m^3$, $K_X = 0.5\,mol/m^3$

Table 5: Channels of the anterior-posterior polarity control network.

3.2 Emergent V_{mem} patterns network

The emergent V_{mem} patterns network describes the spontaneous emergence of non-trivial V_{mem} patterns in a collective of gap junction coupled cells, as presented and analyzed in the main text. Table 6 provides basic information about the substances included in the network model (i.e. substances added in addition to core ions, ATP and ADP that are present by default in all models with information listed in Table 1), Table 7 provides growth and decay expressions for each substance of the network model, and Table 8 provides information about the ion channels included in the network.

All equations for the emergent V_{mem} patterns network model were programmatically generated from mathematical template equations on the basis of user-specified input data in the form of a BETSE configuration file. The configuration file that can be used with BETSE to run the emergent V_{mem} patterns network is supplied as Supporting Information S3.

Substance	**Charge**	**GJ permeable**	**Growth/decay**	D_{GJ} **[m^2/s]**	D_{mem} **[m^2/s]**	**Initial** C_{cell} **[mM]**	**Initial** C_{env} **[mM]**
A	-2	True	True	$1.0e^{-12} - 1.0e^{-13}$	0.0	0.5 (gradient)	0.0
B	0	True	False	$1.0e^{-13}$	0.0	0.5	0.0

Table 6: Substances of the emergent V_{mem} patterns network. The general ions Na^+, K^+, Cl^-, Ca^{2+}, HCO_3^-, P^- , and the substances ATP, ADP and Pi were included in the model, with properties listed in Table 1.

Substance	**Activators**	**Inhibitors**	**Rate Equation**	**Parameters**
A	None	None	$r_A = r_A^{max} - \delta_A [A]$	$r_A^{max} = 1.00e^{-2}$ $\delta_A = 1.00e^{-2}$

Table 7: Growth/decay expressions for the emergent V_{mem} patterns network.

Channel	**Ions**	**Regulation**	**Channel Flux Expression**
K^+ channel	K^+	'A'	$\frac{z_K V_{mem} F P_K^{KChannel}}{R T} \left(\frac{c_K^{cell} - c_K^{env} exp\left(-\frac{z_K V_{mem} F}{RT}\right)}{1 - exp\left(-\frac{z_K V_{mem} F}{RT}\right)} \right)$ $P_K^{KChannel} = P_K^{max} \left(\frac{1}{1 + \left(\frac{[A]}{K_A}\right)^3} \right)$ $P_K^{max} = 1.33e-10\, m/s,\ K_A = 0.5 - 0.75\, mol/m^3$

Table 8: Channels of the emergent V_{mem} patterns network.

References

[1] Pietak A, Levin M. Exploring Instructive Physiological Signaling with the Bioelectric Tissue Simulation Engine. Front Bioeng Biotechnol. 2016;p. 55.

[2] Pekař M. The Thermodynamic Driving Force for Kinetics in General and Enzyme Kinetics in Particular. ChemPhysChem. 2015 Mar;16(4):884–885.

[3] Wessler I, Roth E, Deutsch C, Brockerhoff P, Bittinger F, Kirkpatrick CJ, et al. Release of Non-Neuronal Acetylcholine from the Isolated Human Placenta Is Mediated by Organic Cation Transporters. Br J Pharmacol. 2001 Nov;134(5):951–956.

[4] Wu X, Kekuda R, Huang W, Fei YJ, Leibach FH, Chen J, et al. Identity of the Organic Cation Transporter OCT3 as the Extraneuronal Monoamine Transporter (Uptake2) and Evidence for the Expression of the Transporter in the Brain. J Biol Chem. 1998 Apr;273(49):32776–32786.

[5] Kekuda R, Prasad PD, Wu X, Wang H, Fei YJ, Leibach FH, et al. Cloning and Functional Characterization of a Potential-Sensitive, Polyspecific Organic Cation Transporter (OCT3) Most Abundantly Expressed in Placenta. J Biol Chem. 1998 Jun;273(26):15971–15979.

[6] Vrbjar N, Dzurba A, Ziegelhöffer A. Enzyme Kinetics and the Activation Energy of (Na, K)-ATPase in Ischaemic Hearts: Influence of the Duration of Ischaemia. General physiology and biophysics. 1994;13:405–405.

[7] Costa PF, Emilio MG, Fernandes PL, Ferreira HG, Ferreira KG. Determination of Ionic Permeability Coefficients of the Plasma Membrane of Xenopus Laevis Oocytes under Voltage Clamp. The Journal of physiology. 1989;413:199.

[8] Rose EM, Koo JCP, Antflick JE, Ahmed SM, Angers S, Hampson DR. Glutamate Transporter Coupling to Na,K-ATPase. Journal of Neuroscience. 2009 Jun;29(25):8143–8155.

[9] Lin CH, Lee TH. Sodium or Potassium Ions Activate Different Kinetics of Gill Na, K-ATPase in Three Seawater- and Freshwater-Acclimated Euryhaline Teleosts. Journal of Experimental Zoology Part A: Comparative Experimental Biology. 2005 Jan;303A(1):57–65.

[10] Mackenzie B, Ujwal ML, Chang MH, Romero MF, Hediger MA. Divalent Metal-Ion Transporter DMT1 Mediates Both H+ -Coupled Fe2+ Transport and Uncoupled Fluxes. Pflügers Archiv - European Journal of Physiology. 2006 Jan;451(4):544–558.

[11] Galli A, Petersen CI, deBlaquiere M, Blakely RD, DeFelice LJ. Drosophila Serotonin Transporters Have Voltage-Dependent Uptake Coupled to a Serotonin-Gated Ion Channel. J Neurosci. 1997 May;17(10):3401–3411.

[12] Blackiston D, Adams DS, Lemire JM, Lobikin M, Levin M. Transmembrane Potential of GlyCl-Expressing Instructor Cells Induces a Neoplastic-like Conversion of Melanocytes via a Serotonergic Pathway. Dis Model Mech. 2011;4(1):67–85.

[13] Talley EM, Sirois JE, Lei Q, Bayliss DA. Two-Pore-Domain (Kcnk) Potassium Channels: Dynamic Roles in Neuronal Function. Neuroscientist. 2003 Jan;9(1):46–56.

[14] Koizumi H, Smerin SE, Yamanishi T, Moorjani BR, Zhang R, Smith JC. TASK Channels Contribute to the K+-Dominated Leak Current Regulating Respiratory Rhythm Generation in Vitro. J Neurosci. 2010 Mar;30(12):4273–4284.

[15] Talley EM, Bayliss DA. Modulation of TASK-1 (Kcnk3) and TASK-3 (Kcnk9) Potassium Channels VOLATILE ANESTHETICS AND NEUROTRANSMITTERS SHARE A MOLECULAR SITE OF ACTION. J Biol Chem. 2002 May;277(20):17733–17742.

[16] Horie M, Irisawa H, Noma A. Voltage-Dependent Magnesium Block of Adenosine-Triphosphate-Sensitive Potassium Channel in Guinea-Pig Ventricular Cells. J Physiol. 1987 Jun;387:251–272.

[17] Makary SM, Claydon TW, Enkvetchakul D, Nichols CG, Boyett MR. A Difference in Inward Rectification and Polyamine Block and Permeation between the Kir2.1 and Kir3.1/Kir3.4 K+ Channels. J Physiol. 2005 Nov;568(Pt 3):749–766.

[18] Philipson LH, Hice RE, Schaefer K, LaMendola J, Bell GI, Nelson DJ, et al. Sequence and Functional Expression in Xenopus Oocytes of a Human Insulinoma and Islet Potassium Channel. Proceedings of the National Academy of Sciences. 1991;88(1):53–57.

[19] McKay MC, Worley JF. Linoleic Acid Both Enhances Activation and Blocks Kv1.5 and Kv2.1 Channels by Two Separate Mechanisms. American Journal of Physiology - Cell Physiology. 2001 Oct;281(4):C1277–C1284.

[20] Avery RB, Johnston D. Multiple Channel Types Contribute to the Low-Voltage-Activated Calcium Current in Hippocampal CA3 Pyramidal Neurons. J Neurosci. 1996 Sep;16(18):5567–5582.